Bulut, F., Ben-Zion, Y., Bohnhoff, M. (2012): Evidence for a bimaterial interface along the Mudurnu segment of the North Anatolian Fault Zone from polarization analysis of P waves. - Earth and Planetary Science Letters, 327-328, 17-22

DOI: 10.1016/j.epsl.2012.02.001

Evidence for a bimaterial interface along the Mudurnu segment of the North Anatolian Fault Zone from polarization analysis of P waves

Fatih Bulut[1], Yehuda Ben-Zion[2] and Marco Bohnhoff[1]

1. Helmholtz-Zentrum Potsdam, Deutsches GeoForschungsZentrum, Telegrafenberg, 14473 Potsdam, Germany

2. Department of Earth Sciences, University of Southern California, Los Angeles, CA 90089-0740, USA

Abstract

We present results on imaging contrast of seismic velocities across the Mudurnu segment of the North Anatolian Fault Zone (NAFZ) in northwestern Turkey with polarization analysis of early *P* waveforms generated by near-fault seismicity and recorded by near-fault stations. The analysis uses changes in motion polarity from fault-normal to source-receiver directions to identify early-arriving fault zone head waves on the slow side of the fault, and measure the arrival times of the head and direct *P* waves. The moveout between the head and direct waves with increasing source-receiver distance along the fault provides an estimate of the average contrast of seismic velocities across the fault. The results indicate that the average contrast of *P* wave velocities across the Mudurnu segment of the NAFZ is at least 6%, with the south block being the faster side. The findings provide a basis for deriving improved event locations, focal mechanisms and estimated shaking hazard associated with earthquakes on the fault. The analysis technique can be used in other fault zones monitored with sparse seismic instrumentation.

1. Introduction

Plate boundaries and other major faults have prominent bimaterial interfaces that separate different rock bodies. These are generated progressively by the long-term relative motion of blocks along the faults and the cumulative production of rock damage associated with the faulting process (e.g., Ben-Zion & Sammis, 2003, and references therein). Moreover, large fault zones tend to nucleate along pre-existing sutures between different geological units (e.g., Le Pichon et al., 2005). Field studies show that the active slip zone in large fault structures is often localized along the overall lithology contrast and/or the boundary of a damaged fault zone layer (e.g., Sibson, 2003; Sengor et al., 2005; Dor et al., 2006, 2008; Mitchell et al., 2011).

The existence of bimaterial interfaces in the structure of faults at depth can have important consequences for various aspects of earthquake and fault physics. These include changing dynamically the strength of the fault, suppressing branching of ruptures, reducing the generation of frictional heat, and

producing a statistical preference for propagation direction of earthquakes (e.g., Ben-Zion, 2001). The latter can have strong influence on seismic shaking hazard since rupture directivity can amplify the ground motion in the propagation direction by a factor 3 or more. Contrast of lithology across faults can also significantly affect the geodetic fields during the interseismic periods (e.g. Le Pichon et al., 2005; Wdowinski et al., 2007; Ozeren and Holt, 2010). Ignoring the existence of a velocity contrast across a fault can produce errors in inferred velocity structures and earthquake source properties (e.g., McNally & McEvilly, 1977; Ben-Zion & Malin, 1991; Schulte-Pelkum & Ben-Zion, 2012).

The clearest information on contrast of rock types at seismogenic depth can be obtained from fault zone head waves (FZHW) that spend most of their source-receiver propagation path along the bimaterial fault interface (Ben-Zion, 1989, 1990; Ben-Zion & Malin, 1991). Previous imaging of fault bimaterial interfaces with FZHW used data from dense near-fault seismic arrays (e.g., McGuire & Ben-Zion, 2005; Zhao et al., 2010). In most cases, however, the seismic networks are sparse since they are designed to monitor seismicity on regional scales. Therefore, it is desirable to develop alternative techniques that could be used to detect the existence, and quantify the degree, of velocity contrast across faults. In the present paper we use polarization analysis of seismic phases in early P waveforms to image a bimaterial fault interface in the structure of the Mudurnu segment of the North Anatolian Fault Zone (NAFZ) in northwestern Turkey. The technique may be applied even to data recorded by a single station, so it can have wide applicability.

In the next section we briefly describe the study area and employed data set. In section 3 we present and apply particle motion analysis for detecting FZHW and estimating the velocity contrast across the fault. The analysis indicates that the Mudurnu segment of the NAFZ has a clear bimaterial interface with average velocity contrast of about 6% or more. The results are summarized and discussed in section 4.

2. Tectonic environment and data

The North Anatolian Fault Zone is one of the largest plate-bounding transform faults, separating the Anatolian and Eurasian plates and extending for ~1600 km between Eastern Anatolia and the Northern Aegean. Westward movement of Anatolia has developed in the framework of the northward moving Arabian plate and the Hellenic Subduction Zone where the African lithosphere is subducted below the Aegean. Current right-lateral slip rate along the NAFZ is 20-30 mm/yr (e.g. Barka, 1992, McClusky et al., 2000), repeatedly producing major (M7+) strike-slip earthquakes but also N-S extensional normal faulting events south of the Marmara region. During the 20th century, the NAFZ has ruptured over 900 km of its length (Ambraseys, 1970; Barka, 1999). A series of large earthquakes starting in 1939 near Erzincan in Eastern Anatolia propagated westward towards the Istanbul-Marmara region in North-Western Turkey (Fig

1a).

The two most recent major earthquakes in northwestern Turkey are the 1999 Mw7.4 Izmit and Mw7.1 Düzce events that together ruptured ~200 km of the NAFZ east of the Marmara region (e.g. Barka et al., 2002). Both main shocks had a dextral strike-slip mechanism reflecting the overall characteristic of the NAFZ. The Izmit earthquake occurred on August 17, 1999 with rupture extending from the eastern Sea of Marmara to the Düzce area. The subsequent Düzce event occurred 87 days later (November 12, 1999) extending the Izmit rupture by another 50 km to the East (Fig 1).

In this study we investigate the velocity contrast across the Mudurnu segment of the NAFZ using data recorded by a station (CAY) located a few km on the north side of the fault (Fig. 1b). The station is part of the GTF (German TaskForce for earthquakes, Baumbach et al., 2003) and SABONET (C. Milkereit, pers. comm.) seismic networks. The Mudurnu segment branches off the Izmit segment and continues eastward parallel and south to the Düzce branch. It represents the southern boundary of the Almacık Block and ruptured most recently during the 1967 M7.1 Mudurnu event (Ambraseys and Zatopek, 1969). The seismograms are sampled at 100 Hz and recorded in a triggered mode except for the time period of the 1999 Izmit-Düzce aftershock activity (17.08-12.12.1999).

3. Analysis

Earthquakes on a fault consisting of a bimaterial interface generate FZHW that spend a large portion of their propagation paths refracting along the bimaterial interface (Ben-Zion, 1989, 1990). The head waves propagate along the bimaterial interface with the velocity and motion polarity of the faster block, and are radiated from the fault to the slower velocity side where they are characterized by an emergent waveform with opposite motion polarity to that of the direct body waves. The FZHW are the first arriving phases at locations on the slower block with normal distance to the fault less than a critical distance x_c given (Ben-Zion, 1989) by

$$x_c = r \cdot \tan\left[\cos^{-1}\left(\alpha_2 / \alpha_1\right)\right] \tag{1}$$

where r is the total propagation distance along the fault (both along-strike and up-dip direction) and α_2 and α_1 are the average P wave velocities of the slower and faster media, respectively. For an interface between two different quarter spaces, the differential arrival time (Δt) between first arriving head wave and the following direct P wave grows with the distance traveled along the fault (r) as

$$\Delta t \sim r\left(\frac{1}{\alpha_2}-\frac{1}{\alpha_1}\right)\sim r\left(\frac{\Delta\alpha}{\alpha^2}\right) \tag{2}$$

with α and $\Delta\alpha$ denoting the average and differential P waves velocities, respectively (Ben-Zion & Malin, 1991). If an average P wave velocity can be estimated, it can be used along with the gradient of the differential arrival time versus propagation distance curve to obtain a first order approximation for the strength of the velocity contrast ($\Delta\alpha$) across the fault.

FZHW are radiated to the slow side of the fault from the bimaterial interface, in contrast to the direct body waves that are radiated from the source back-azimuth direction (Fig 2a). This can be utilized to detect FZHW with polarization analysis and measure their arrival time and duration. In this paper we use particle motions of P waves in the early portions of earthquake-generated seismograms to track the variation between the incoming directions of FZHW and direct P wave arrivals at a near-fault station. This is done by incrementally calculating the directions of the P waves using horizontal displacement recordings subdivided into 0.1 s long time windows (Fig. 2b).

Following Jurkevic (1988), the polarization ellipse is computed within moving time windows by solving the eigenproblem for the covariance matrix. Let X represent one of the three-components (Z, N, E) zero mean displacement data in a time window. The covariance matrix is computed as:

$$S=\frac{\mathbf{X}\mathbf{X}^T}{N} \tag{3}$$

where N is the number of samples. The principal axes of the polarization ellipsoid are found by solving the eigenproblem for the covariance matrix $\boldsymbol{S}$. The eigenvalues ($\lambda_1,\lambda_2,\lambda_3$) and eigenvectors ($\mathbf{u}_1,\mathbf{u}_2,\mathbf{u}_3$) give three principal ellipsoid axes by $\lambda_j\mathbf{u}_j$ (j=1,.,3), where the eigenvectors are axis orientations and eigenvalues are their amplitudes. The direction of incoming P wave (Az) is assumed to be the horizontal orientation of rectilinear motion corresponding to the eigenvector of the largest eigenvalue ($\mathbf{u}_1$):

$$Az=\tan^{-1}\left(\frac{u_{21}}{u_{31}}\right) \tag{4}$$

Moving-window polarization analysis can be used to pick the time when the incoming P waves are rotated from fault-normal direction into the source azimuth. This time provides an estimate for the transition from

FZHW to direct P waves. Fig. 2 illustrates how the polarization of the early P waveform at station CAY about 1.5 km to the north of the NAFZ changes as expected for the transition from a FZHW to a direct body wave. We note that typical significant damage zone in the immediate vicinity and top few km of the fault (e.g. Ben-Zion et al., 2003; Lewis and Ben-Zion, 2010) is not expected to affect the early P waveforms generated by the employed earthquakes (depth ≥ 10 km) and recorded at stations outside the damage zone (e.g. McGuire and Ben-Zion, 2005). The polarization analysis employs moving time windows of 0.1 s plus one additional sample on each side. As discussed below, similar changes of polarizations from fault-normal to the epicenter direction are obtained for other waveforms recorded at station CAY. The results imply that the NE side of the NAFZ along the Mudurnu segment has lower seismic velocities.

As a proof-of-concept, we apply the same polarization analysis to data from the Parkfield section of the San Andreas Fault (SAF) known to include fault zone head waves (e.g. Ben-Zion and Malin, 1991). We use as examples waveforms recorded at station MMNB on the slow side of the SAF (Fig. 3a) that were analyzed recently by Zhao et al. (2010). Particle motions for the initial P wave windows exhibit fault-normal direction of incoming waves, which turn around 0.2 sec into a NW-SE orientation pointing to the source azimuth (Fig. 3b). Similar results are obtained with other waveforms shown by Zhao et al. (2010) to include FZHW in the early portions of seismograms. The results confirm the utility of our polarization analysis for detecting and measuring the duration of FZHW.

Fig. 4 presents results based on polarization analysis using three-component data of 24 events recorded at station CAY. We use events with locations (Bulut et al., 2007) within 5 km normal distance from the main fault branch, depth ≥ 10 km, source-station distances less ≤ 25 km, and waveforms with signal-to-noise ratios ≥ 20 (Fig. 4b). A moving window sliding by one sample (0.01 s) is used to achieve the highest possible precision. Polarization analysis as illustrated in Figs. 2 and 3 is performed to measure the arrival times of FZHW and direct P arrivals (Fig. 4a). Aligning the seismograms on the FZHW arrivals and plotting the results versus hypocentral distance is used to measure a move-out as a function of time delay between P_{DIRECT} and P_{FZHW}. The results indicate a coherent velocity contrast along the fault in the study area. The slope of the move-out is proportional (Eq. 2) to the average velocity contrast in the fault section containing the events. Fitting a regression line to the differential travel times in Fig. 4a gives an average velocity contrast along the imaged fault segment of 6.2% (err: ±0.7%).

4. Discussion

Fault zone head waves provide direct evidence for the existence of bimaterial fault interfaces and high-resolution tool for imaging the velocity contrast across the fault (e.g. Ben-Zion et al., 1992; Lewis et al., 2007; Zhao et al., 2010). Previous imaging studies based on FZHW employed dense small-aperture seismic

arrays across the fault section of interest. However, typical seismic networks are designed to monitor seismicity at large (regional) scale and they usually lack sufficient station density to detect and analyze FZHW with the previously employed techniques.

In the present study we show that particle motion analysis of early *P* waveforms, performed on records of a single three-component seismograph located slightly off the target fault segment on the slower crustal block, can be used to detect FZHW and measure the arrival times of the head and direct *P* waves. The moveout between the head and direct waves associated with different events on the fault provides a simple tool for estimating the average velocity contrast across the fault. The analysis procedure can be used for detecting FZHW and investigating the velocity contrast across other faults that are not instrumented with dense local arrays. Recently, Ozakin et al. (2012) used teleseismic arrivals at stations near the NAFZ to estimate the velocity contrast across the rupture zone of the 1944 Gerede earthquake east of Ismetpasa. That technique does not require seismicity on the fault, but it provides less accurate and direct results on the existence of a fault bimaterial interface than our particle motion analysis and other techniques using FZHW.

The analysis of particle motion with moving time windows produces some limitations on the accuracy of estimating the phase arrivals and time delays between the FZHW and direct *P* waves. Here we use moving time windows that are partly overlapping by 7 sampling points. The overlaps reduce somewhat the rectilinearity of particle motions in the transitions between the FZHW and direct *P* wave. This depends on the signal-to-noise ratio of the FZHW and direct arrivals as well as on the station-event distance. The length of the moving windows could be adjusted to fine-tune the accuracy of the time delay measurements. The window length should include at least two cycles of the particle motion to enable deriving the direction of propagating waves. This depends on the frequency content and sampling rate of the analyzed data. In our case, we used 0.1 s long windows for *P* wave recordings associated with sampling rate of 100 Hz and dominant frequency content in the range 20-40 Hz.

Şengör et al. (2005) and Le Pichon et al. (2005) discuss evidence for lithology contrast across the NAFZ based on geological and geodetic investigations. Our study area is bounded by two E-W oriented sub-parallel segments of the NAFZ that failed during the 1967 Mudurnu and 1999 İzmit earthquakes (Fig. 1). Our analysis applies to the easternmost section of the 1967 rupture zone that forms a geological boundary between the Akyazi Basin in the north and the Anatolian Plate in the south (Barka et al., 2002). The velocity contrast imaged in this work likely represents the structural difference between the basin (and its underlying formation) and the Anatolian Plate.

Several 3-D crustal models have been developed for our study area using data from magnetotelluric experiments and travel time tomography from local earthquakes. Despite considerable differences in

resolved scales, it is informative to compare results from those studies with those derived in the present paper. Tomography images of Nakamura et al. (2002) and Baris et al. (2005) indicate that the crust in northwestern Turkey has a velocity contrast over the top ~7 km of up to 6%. The Vp and Vs perturbations confirm that the Mudurnu segment represents a boundary between a faster block to the south and a slower block to the north. The velocity contrast is not apparent in the tomography images below 7 km. Analysis of magnetotelluric data indicates (Kaya et al., 2009) a similar boundary across the NAFZ between high and low conductivity blocks, with high conductivity in the north and low conductivity in the south. Our approach allows imaging directly the velocity contrast across the fault, rather than properties of the adjacent crustal blocks, therefore providing complementary information for quantifying the fault bimaterial interface. The above studies and the results of the present work, associated with completely independent data and techniques, consistently indicate that the Mudurnu segment of the NAFZ represents a boundary between significantly different crustal units.

Dor et al. (2008) inferred from observed asymmetry of rock damage across the rupture zone of the 1944 earthquake on the NAFZ that the north side of the fault has faster seismic velocity at seismogenic depth. This was based on the assumption that the damage asymmetry was produced by statistically-preferred propagation direction of large earthquakes on the fault (Ben-Zion and Shi, 2005). The imaging results of Ozakin et al. (2012) are consistent with the inference of Dor et al. (2008). These set of studies indicate that large earthquakes on that section of the NAFZ tend to propagate, and hence produce larger shaking hazard, to the west. Our results on the velocity contrast across the Mudurnu segment with higher velocity to the south imply a reversal in the sense of the velocity contrast between the 1967 and 1944 large (M7+) earthquake rupture zones. This can produce a dynamic arrest mechanism for earthquakes propagating from either zone to the other, as reversal of velocity contrast increases the normal stress at the tip of propagating ruptures (e.g. Weertman, 1980; Ben-Zion, 2001).

Our imaging results on the existence of a clear velocity contrast across the Mudurnu segment of the NAFZ, with average value over the section sampled by the employed data of at least 6%, provide a basis for deriving more accurate event locations and focal mechanisms in future analyses of earthquakes on the fault. The results in conjunction with models of bimaterial ruptures suggest that earthquakes on the Mudurnu segment have statistically-preferred propagation direction to the east. This should be tested by future analyses of asymmetry of rock damage across the fault (e.g. Dor et al., 2008; Mitchell et al., 2011), along with directivity and along-strike symmetry properties of small earthquakes as done recently by Zaliapin & Ben-Zion (2011) and Lengline & Got (2011) in the context of large faults in California.

Acknowledgement

We thank the German Task Force for earthquakes of GFZ, in particular J. Zschau, E. Günther and C. Milkereit, for sharing the seismic recordings from the joint SABONET network. We also thank Peter Shearer for constructive comments. The study was funded by the Helmholtz Foundation in the frame of Young Investigators Group "From Microseismicity to Large Earthquakes". YBZ acknowledges support from the Alexander von Humboldt foundation.

References

Ambraseys, N.N., 1970. Some characteristic features of the North Anatolian fault zone into the north Aegean. Tectonophysics, 9, 143-165.

Ambraseys, N. N. and Zatopek, A. 1969. The Mudurnu Valley earthquake of July 22nd 1967, Bull. Seism. Soc. Am., 59, 521-589.

Baris S., Nakajima J., Hasegawa A., et al., Three-dimensional structure of Vp, Vs, and Vp/Vs in the upper crust of the Marmara region, NW Turkey. Earth Planets and Space 57 (11): 1019-1038 2005

Barka, A., 1992. The North Anatolian Fault, Ann. Tectonicae, 6, 164-195.

Barka, A., 1999. The 17 August Izmit earthquake. Science, 285, 1858-1859.

Barka, A. and 21 others, 2002. The Surface Rupture and Slip Distribution of the 17 August 1999 Izmit Earthquake (M 7.4), North Anatolian Fault. Bull. Seism. Soc. Am., 92(1), 43-60.

Ben-Zion, Y., 1989, The response of two joined quarter spaces to SH line sources located at the material discontinuity interface, Geophys. J. Int., 98, 213-222.

Ben-Zion, Y., 1990, The response of two half spaces to point dislocations at the material interface, Geophys. J. Int., 101**,** 507-528.

Ben-Zion, Y., 2001. Dynamic Rupture in Recent Models of Earthquake Faults, J. Mech. Phys. Solids, **49**, 2209-2244.

Ben-Zion, Y. and P. Malin, 1991. San Andreas fault zone head waves near Parkfield, California, Science, **251**, 1592-1594.

Ben-Zion, Y., S. Katz and P. Leary, 1992. Joint inversion of fault zone head waves and direct P arrivals for crustal structure near major faults, *J. Geophys. Res,* **97**, 1943-1951.

Ben-Zion, Y., Z. Peng, D. Okaya, L. Seeber, J. G. Armbruster, N. Ozer, A. J. Michael, S. Baris and M. Aktar, [2003.] A shallow fault zone structure illuminated by trapped waves in the Karadere-Duzce branch of the North Anatolian Fault, western Turkey, *Geophys. J. Int.*, **152**, 699-717.

Ben-Zion, Y., C. G. Sammis, 2003. Characterization of Fault Zones , Pure Appl. Geophys., 160, 677-715.

Ben-Zion, Y. and Shi, Z., 2005. Dynamic rupture on a material interface with spontaneous generation of

plastic strain in the bulk. *Earth. Plant. Sci. Lett.*, 236, 486-496, DOI: 10.1016/j.epsl.2005.03.025.

Bulut, F., Bohnhoff M., Aktar M. and Dresen G. (2007), Characterization of aftershock-fault plane orientations of 1999 Izmit (Turkey) earthquake using high-resolution aftershock locations, Geophys. Res. Lett., Vol.34, L20306, doi: 10.1029/2007GL031154.

Dor O., T. K. Rockwell and Y. Ben-Zion, Geologic observations of damage asymmetry in the structure of the San Jacinto, San Andreas and Punchbowl faults in southern California: A possible indicator for preferred rupture propagation direction, Pure Appl. Geophys., 163, 301-349, DOI 10.1007/s00024-005-0023-9, 2006.

Dor, O., Yildirim, C., Rockwell, T.K., Ben-Zion, Y., Emre, O., Sisk, M., Duman, T. Y., 2008, Geologic and geomorphologic asymmetry across the rupture zones of the 1943 and 1944 earthquakes on the North Anatolian Fault: possible signals for preferred earthquake propagation direction, Geophys. J. Int., **173,** 483–504, doi: 10.1111/j.1365-246X.2008.03709.x.

Jurkevics, A. 1988. Polarization analysis of three-component array data, Bull. Seism. Soc. Am., 78, 1725-1743.

Kaya, T, Tank, SB, Tuncer, MK , Rokoityansky, II , Tolak, E, Savchenko, T, 2009, Asperity along the North Anatolian Fault imaged by magnetotellurics at Duzce, Turkey, EARTH PLANETS AND SPACE, 61 871-884 2009.

Lengline, O. & Got, J.-L., 2011. Rupture Directivity of Micro-Earthquake Sequences near Parkfield, California, *Geophys. Res. Lett.*, 38, L08310, doi:10.1029/2011GL047303.

Lewis, M.A, Y. Ben-Zion and J. McGuire, 2007, Imaging the deep structure of the San Andreas Fault south of Hollister with joint analysis of fault-zone head and direct *P* arrivals, *Geophys. J. Int.*, **169,** 1028–1042, doi: 10.1111/j.1365-246X.2006.03319.x.

Lewis, M. A. and Y. Ben-Zion, 2010, Diversity of fault zone damage and trapping structures in the Parkfield section of the San Andreas Fault from comprehensive analysis of near fault seismograms, *Geophys. J. Int.*, **183**, 1579-1595, doi: 10.1111/j.1365-246X.2010.04816.x.

Le Pichon, X., C. Kreemer, and N. Chamot-Rooke (2005), Asymmetry in elastic properties and the evolution of large continental strike-slip faults, J. Geophys. Res., 110, B03405, doi:10.1029/2004JB003343.

McClusky, S. et al., 2000, Global Positioning System constraints on plate kinematics and dynamics in the eastern Mediterranean and Caucasus, J. Geophys. Res., 105, 5695-5719.

McGuire, J. and Y. Ben-Zion, 2005, High-resolution imaging of the Bear Valley section of the San Andreas Fault at seismogenic depths with fault-zone head waves and relocated seismicity, Geophys. J. Int., 163, 152-164, doi: 10.1111/j.1365-246X.2005.02703.x.

McNally, K. C. and T. V. McEvilly (1977), Velocity contrast across the San Andreas Fault in central California, small-scale variations from *P*-wave nodal plane distortion, *Bull. Seismol. Soc. Am.*, 67, 1565–1576.

Mitchell, T. M., Y. Ben-Zion and T. Shimamoto, 2011, Pulverized Fault Rocks and Damage Asymmetry along the Arima-Takatsuki Tectonic Line, Japan, *Earth Planet. Sci. Lett.*, doi:10.1016/j.epsl.2011.04.023.

Nakamura, A., A. Hasegawa, A. Ito, B. Üçer, S. Baris, Y. Honkura, T. Kono, S. Hori, R. Pektas, T. Komut, C. Çelik, and A. M. Isikara (2002). P-wave velocity structure of the crust and its relationship to the occurrence of the 1999 Izmit, Turkey, earthquake and aftershocks, Bull. Seism. Soc. Am. 92, no. 1, 330-338.

Ozakin, Y., Y. Ben-Zion, M. Aktar, H. Karabulut and Z. Peng, 2012. Velocity contrast across the 1944 rupture of the North Anatolian fault east of Ismetpasa from analysis of teleseismic arrivals, *Geophys. Res. Lett.*, in review.

Özeren, S. and W. E. Holt, 2010, The dynamics of the eastern Mediterranean and eastern Turkey, Geophys. J. Int., **183,** 1165–1184.

Schulte-Pelkum, V. and Y. Ben-Zion, 2012. Apparent vertical Moho offsets under continental strike-slip faults from lithology contrasts in the seismogenic crust, *Geophys. J. Int.*, in review.

Sengor, A.M.C., O. Tuysuz, C. Imren, M. Saknc¸ H. Eyidogan, N. Gorur, X. Le Pichon, and C. Rangin (2005), The North Anatolian Fault: A New Look, Annu. Rev. Earth Planet. Sci., 33, 37-112, doi: 10.1146/annurev.earth.32.101802.120415.

Sibson, R. H. (2003), Thickness of the seismic slip zone, Bull. Seism. Soc. Am., 93, 1169-1178.

Wdowinski S., B. Smith-Konter, Y. Bock, and D. Sanwell (2007), Diffuse interseismic deformation across the Pacific-North America plate boundary, Geology, **35(4)**, 311–314.

Weertman, J., 1980, Unstable slippage across a fault that separates elastic media of different elastic constants, *J. Geophys. Res*., 85, 1455-1461.

Zaliapin, I. and Y. Ben-Zion, 2011, Asymmetric distribution of aftershocks on large faults in California, *Geophys. J. Int.*, doi: 10.1111/j.1365-246X.2011.04995.x.

Zhao, P., Z. Peng, Z. Shi, M. Lewis and Y. Ben-Zion, 2010, Variations of the Velocity Contrast and Rupture Properties of M6 Earthquakes along the Parkfield Section of the San Andreas Fault, Geophys. J. Int., doi: 10.1111/j.1365-246X.2009.04436.x, **180**, 765–780.

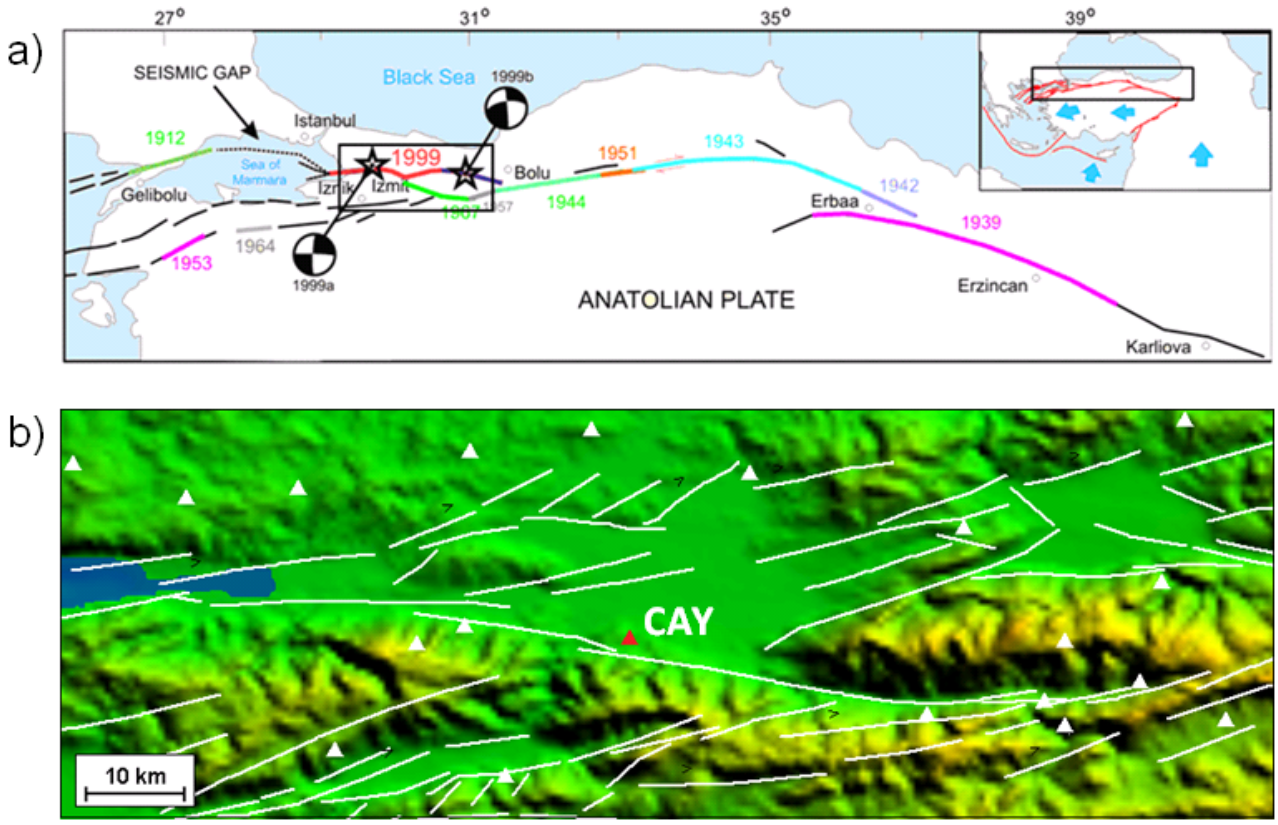

Fig 1 (a) Large earthquake ruptures along the North Anatolian Fault Zone during the 20th century. The study area is indicated by the rectangle. Numbers give the years of M7+ events since 1912 with 1999a and 1999b corresponding to the Izmit and Düzce events, respectively. The inset in the upper right shows the broader region. (b) Enlarged part of the box in (a). The red triangle marks the seismic station (CAY) used in this study and white triangles are additional stations of the joint GTF/SABONET network (Baumbach et al., 2003; C. Milkereit, pers. comm.). The background colors indicate topography with yellow and green denoting highs and lows, respectively. The white lines mark surface traces of presently active faults.

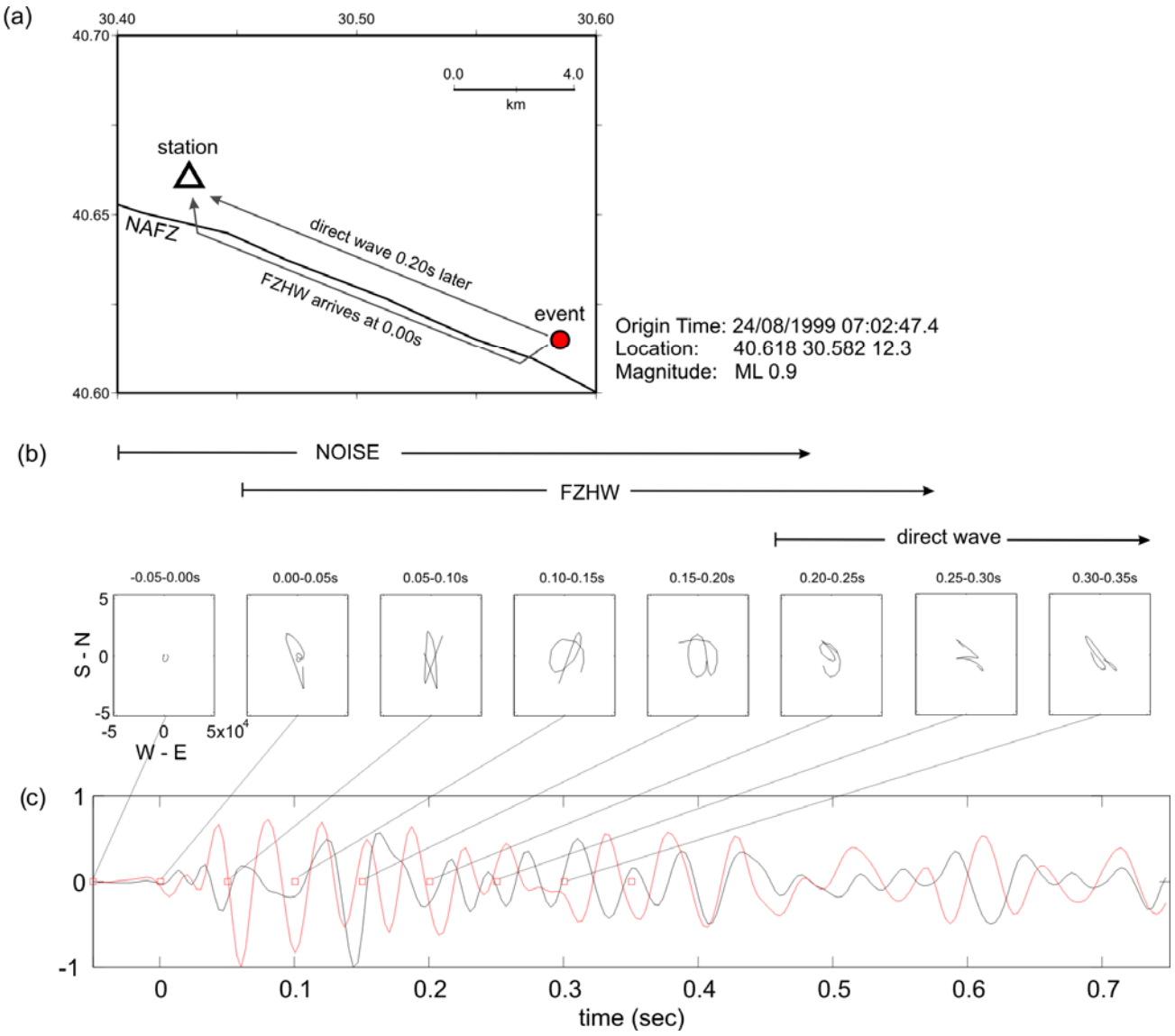

Fig 2. Illustration of particle motion analysis using example seismograms from the NAFZ: (a) Event-station layout and the fault-ray path configuration. The triangle and dot indicate, respectively, the locations of seismic station CAY on the north side of the fault and a near-fault earthquake southeast of the station. (b) Azimuth variations of incoming P-waves based on horizontal recordings at seismograph CAY. The numbers at the upper right corners at each box indicate the starting of 0.05 s time windows used in the polarization analysis. Following the initial time windows with noise, the particle motions show N-S oriented polarizations (0.00 – 0.20 s) consistent with radiation from the fault generated by a P-wave traveling along a velocity-contrast interface (FZHW). In the time interval (0.20 – 0.35 s), the polarizations turn into a NW-SE orientation consistent with the theoretical ray-path of the direct P body waves. (c) Horizontal recordings (N-S component red and E-W component black) used for the polarization analysis.

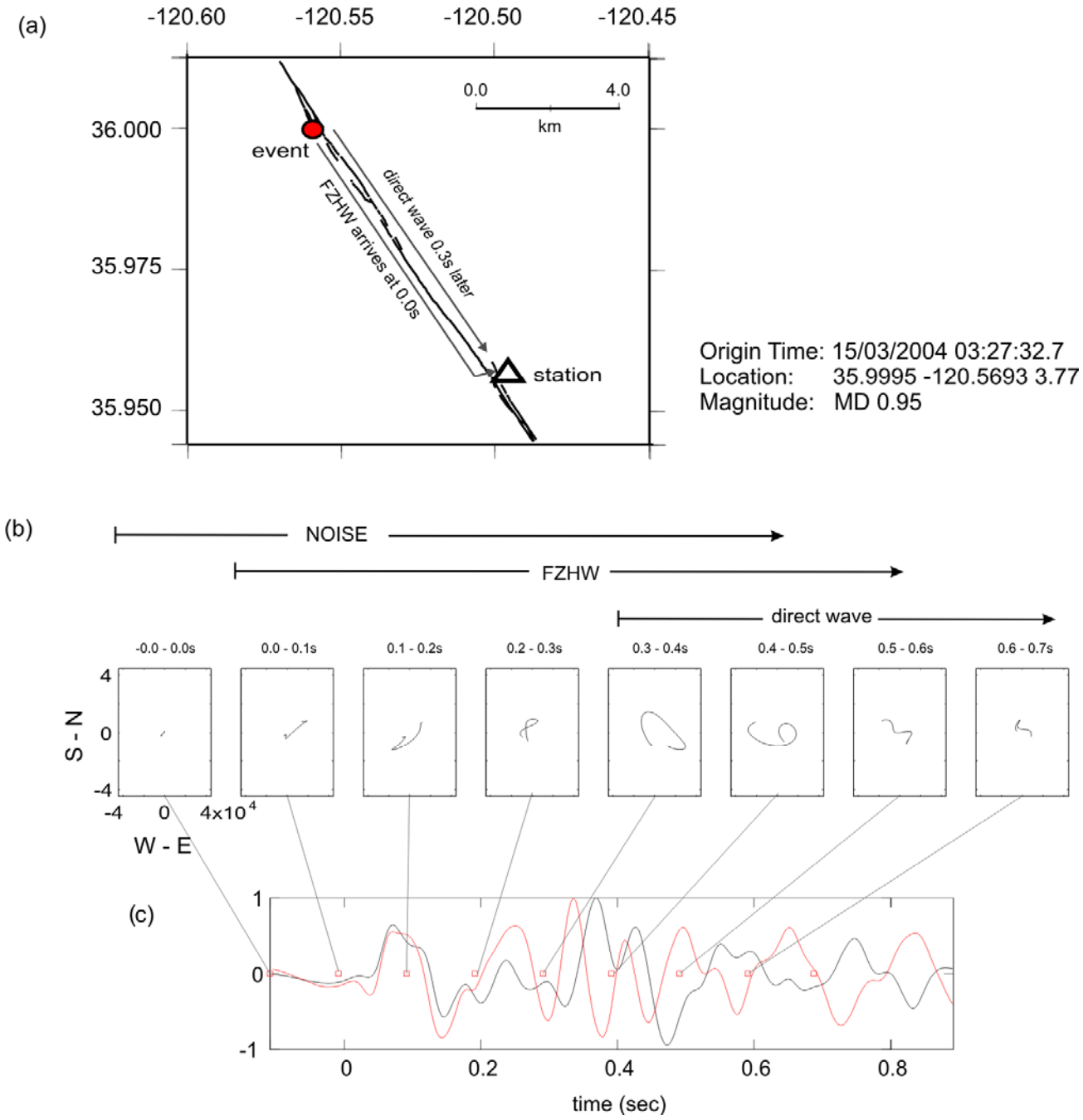

Fig 3. Illustration of particle motion analysis with example seismograms recorded by station MMNB near the Parkfield section of the San Andreas Fault: The symbols and notations are similar to those used in Fig. 2. The seismograms start with a clear FZHW analyzed previously by Zhao et al. (2010). The change of polarization from an initial fault-normal direction to back-azimuth direction to the source confirms the utility of the particle motion analysis to detect FZHW and measure the time separation between that phase and the direct P arrival. (c) Horizontal recordings (N-S component red and E-W component black) used for the polarization analysis.

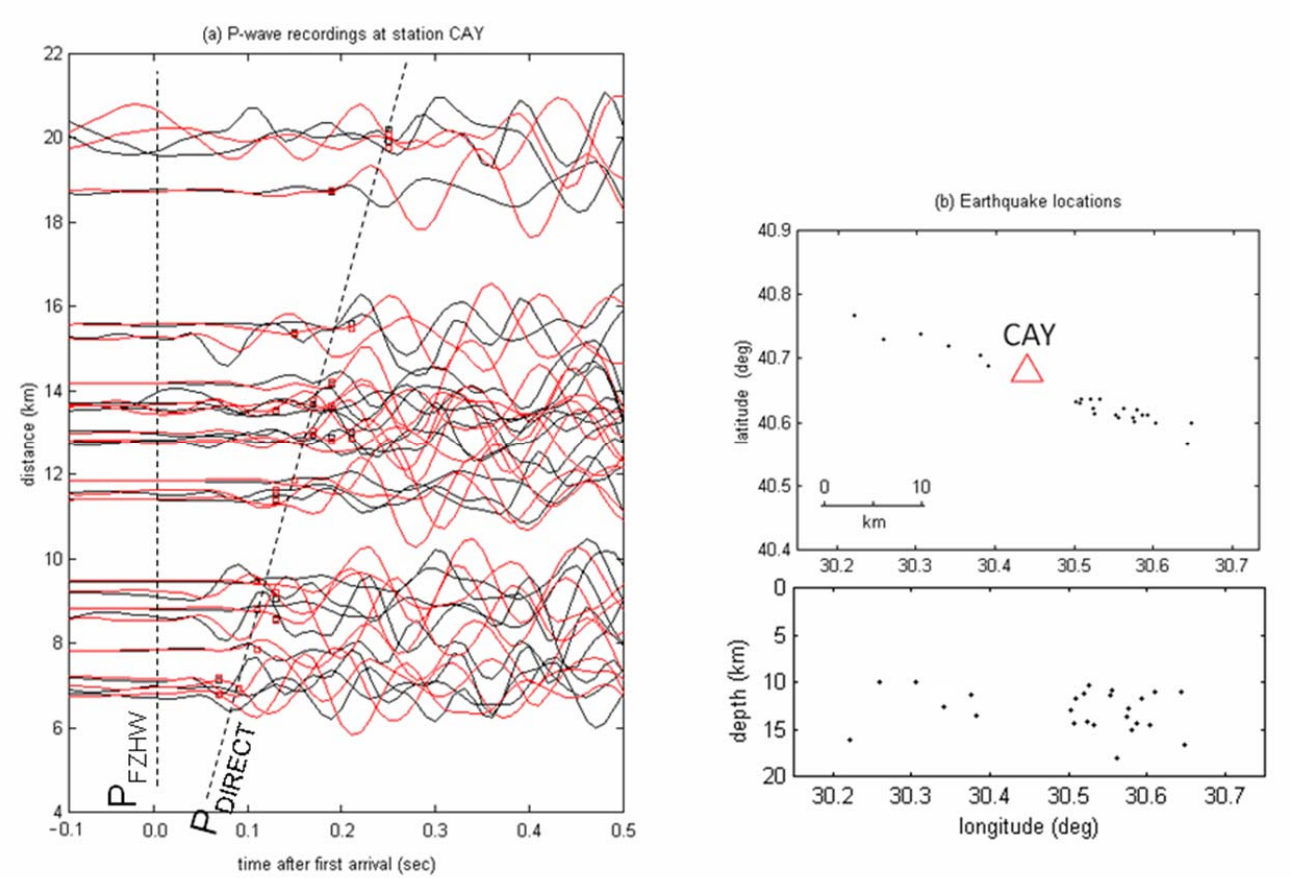

Fig 4 (a) Horizontal P- waveforms recorded at station CAY located ~1.5 km from the surface trace of the NAFZ (red N-S component and black E-W component). The waveforms are aligned on the times of transitions from noise to fault-normal polarization directions indicating the arrivals of FZHW (see Figs. 2-3 and text for analysis details). The red and black markers show the arrivals of the direct P body waves determined from the polarization analysis. (b) Epicentral (top panel) and depth (bottom panel) distribution of the near-fault earthquakes used in the analysis.